7156 *Inorg. Chem.* **2010**, *49*, 7156–7164
DOI: 10.1021/ic100981c

Inorganic Chemistry
Article

Polyfluoride Anions, a Matrix-Isolation and Quantum-Chemical Investigation

Sebastian Riedel,*,† Tobias Köchner,† Xuefeng Wang,‡ and Lester Andrews§

†*Institut für Anorganische und Analytische Chemie, Albert-Ludwigs Universität Freiburg, Albertstrasse 21, D-79104 Freiburg im Breisgau, Germany,* ‡*Chemistry Department, Tongji University, Shanghai 200092, China, and* §*Department of Chemistry, University of Virginia, Charlottesville, Virginia 22904-4319*

Received May 17, 2010

Laser-ablation experiments with metals provide a source of electrons for capture processes, which are codeposited with solid argon and neon containing molecular fluorine. New argon and neon matrix absorptions at 510.6 and 524.7 cm^{-1}, respectively, are photosensitive upon irradiation at >290 nm, which is consistent with their assignment to an isolated anion. These bands are below the $[M]^+[F_3]^-$ antisymmetric trifluoride stretching frequency of 550 cm^{-1} in an argon matrix, which is the typical relationship for cation−anion complexes and matrix-isolated anions. Thus, we report the isolated $[F_3]^-$ anion in solid argon and neon environments. Moreover, we have carried out quantum-chemical calculations up to and including the CCSD(T) method to investigate the stabilities of polyfluoride anions higher than the $[F_3]^-$ anion.

Introduction

Several polyhalogen anions are well-known experimentally,[1−4] and especially the trihalide anions $[X_3]^-$ (X = F, Cl, Br, I) are of wider interest and practical use for superconductivity,[5−7] organic synthesis,[8,9] and polymer science.[10] These trihalide anions are dominated by the heavier halogens iodine and bromine, with a decreasing number of anions involving fluorine. Only one polyfluoride anion was initially observed first under cryogenic conditions in an argon matrix as $[M]^+[F_3]^-$ (M = K, Rb, Cs) complexes[11,12] and later in the gas phase by mass spectrometry.[13,14] This species has generated considerable synthetic and theoretical interest. Numerous quantum-chemical calculations have been done to investigate the chemical bonding, stability, and properties of the $[F_3]^-$ anion.[13−24] These computational studies have shown that an adequate description of the $[F_3]^-$ anion requires very sophisticated quantum-chemical treatment. This can be exemplified by a comparison of the $[F_3]^- \rightarrow [F]^- + F_2$ dissociation energy where MCSCF gives 53 kJ mol^{-1} and density functional theory (BLYP) gives 197 kJ mol^{-1}. The best agreement between the experimentally measured dissociation energy (98.4 ± 10.6 kJ mol^{-1})[14] is given by CCSD(T) calculations (103 kJ mol^{-1}).[17] Both values agree very well and show the $[F_3]^-$ anion to be rather stable in the gas phase.

Here we report the first observation of the isolated $[F_3]^-$ anion stabilized under cryogenic conditions. This species is formed by electron capture processes from laser-ablated metals with molecular fluorine in excess argon and neon during condensation at 4 K. The $[F_3]^-$ ion has been characterized and investigated by IR spectroscopy and quantum-chemical calculations up to and including the CCSD(T) method. Moreover,

*To whom correspondence should be addressed. E-mail: sriedel@psichem.de. Fax: ++49 761 203-6001.

(1) Holleman, A. F.; Wiberg, E. *Lehrbuch der Anorganischen Chemie*; Walter de Gruyter: Berlin, 2007; Vol. *102*, p 1209.
(2) Housecroft, C. E.; Sharpe, A. G. *Inorganic Chemistry*, 3rd ed.; Pearson Education Ltd.: Essex, U.K., 2008.
(3) Klapötke, T. M.; Tornieporth-Oetting, I. C. *Nichtmetallchemie*; VCH: Weinheim, Germany, 1994.
(4) Steudel, R. *Chemie der Nichtmetalle*; Walter de Gruyter: Berlin, 1998.
(5) Williams, J. M.; Wang, H. H.; Emge, T. J.; Geiser, U.; Beno, M. A.; Leung, P. C. W.; Carlson, K. D.; Thorn, R. J.; Schultz, A. J.; Whangbo, M. H. *Prog. Inorg. Chem.* **1987**, *35*, 51–218.
(6) Williams, J. M.; Ferraro, J. R.; Thorn, R. J.; Carlson, U.; Geiser, H. H.; Wang, A. M.; Kini, A. M.; Whagbo, M. H. *Organic Superconducters*; Prentice Hall: Englewood Cliffs, NJ, 1992.
(7) Ishiguro,T.; Yamaji, K. *Organic Superconductors*; Springer Series in Solid-State Sciences 88; Springer: Berlin, 1990; p 288.
(8) Stang, P. J.; Zhdankin, V. V. *Chem. Rev.* **1996**, *96*, 1123–1178.
(9) Schlama, T.; Gabriel, K.; Gouverneur, V.; Mioskowski, C. *Angew. Chem., Int. Ed.* **1997**, *36*, 2342–2344.
(10) Harada, I.; Furukawa, Y.; Tasumi, M.; Shirakawa, H.; Ikeda, S. *J. Chem. Phys.* **1980**, *73*, 4746–4757.
(11) Ault, B. S.; Andrews, L. *J. Am. Chem. Soc.* **1976**, *98*, 1591–1593.
(12) Ault, B. S.; Andrews, L. *Inorg. Chem.* **1977**, *16*, 2024–2028.
(13) Tuinman, A. A.; Gakh, A. A.; Hinde, R. J.; Compton, R. N. *J. Am. Chem. Soc.* **1999**, *121*, 8397–8398.
(14) Artau, A.; Nizzi, K. E.; Hill, B. T.; Sunderlin, L. S.; Wenthold, P. G. *J. Am. Chem. Soc.* **2000**, *122*, 10667–10670.
(15) Cahill, P. A.; Dykstra, C. E.; Martin, J. C. *J. Am. Chem. Soc.* **1985**, *107*, 6359–6362.
(16) Ewig, C. S.; Van Wazer, J. R. *J. Am. Chem. Soc.* **1990**, *112*, 109–114.
(17) Heard, G. L.; Marsden, C. J.; Scuseria, G. E. *J. Phys. Chem.* **1992**, *96*, 4359–4366.
(18) Kar, T.; Sanchez Marcos, E. *Chem. Phys. Lett.* **1992**, *192*, 14–20.
(19) Wright, T. G.; Lee, E. P. F. *Mol. Phys.* **1993**, *79*, 995–1009.
(20) Malcolm, N. O. J.; McDouall, J. J. W. *J. Phys. Chem.* **1996**, *100*, 10131–10134.
(21) Mota, F.; Novoa, J. J. *J. Chem. Phys.* **1996**, *105*, 8777–8784.
(22) Tozer, D. J.; Sosa, C. P. *Mol. Phys.* **1997**, *90*, 513–524.
(23) Czernek, J.; Zivny, O. *J. Chem. Phys.* **2008**, *129*, 194305/194301–194305/194304.
(24) Braida, B.; Hiberty, P. C. *J. Phys. Chem. A* **2008**, *112*, 13045–13052.

 Published on Web 07/01/2010

we have investigated the stabilities of the polyfluoride anions $[F_4]^-$ and $[F_5]^-$ at the coupled-cluster level.

Experimental Section

The technique for laser ablation and FTIR matrix investigation has been described previously.[25,26] The metals were mounted on a rotating (1 rpm) stainless steel rod. The Nd:YAG laser fundamental (1064 nm, 10 Hz repetition rate, 10 ns pulse width, 10−20 mJ pulses) was focused on the target through a hole in the CsI cryogenic window (maintained at 4−6 K). Metal atoms were codeposited with 0.5−4% F_2 in argon and neon at 3−4 mmol h^{-1} for 1 h periods. Commercial fluorine (Matheson) was handled in a dedicated, well-passivated stainless steel manifold and spray-on line. Our 1 L fluorine reservoir was cooled to 77 K during preparation of the matrix sample to retain most of the common impurity molecules in commercial fluorine (the deposited samples contained SiF_4 impurity at 1023 cm^{-1} with 0.01 absorbance). FTIR spectra were recorded with an accuracy of 0.1 cm^{-1} on a Nicolet 750 spectrometer at 0.5 cm^{-1} resolution. Matrix samples were successively warmed and recooled, and more spectra were collected; the matrix was subjected to broad-band photolysis with a mercury arc street lamp (Sylvania H39 KB-175) with the globe removed (> 220 nm) at different stages in the annealing cycles.

Molecular structures were optimized at the density functional theory (DFT) level (with B3LYP[27−30] and BP86[31,32] functionals), Møller−Plesset perturbation theory (MP2), and coupled-cluster CCSD, with the CCSD(T) level using the programs *Gaussian03*[27] for the DFT and *Molpro 2006.1*[33] (structure optimizations) and *ACESII*[34] (calculation of frequencies) for ab initio calculations. Higher-order coupled-cluster excitations like CCSDT have been performed by *MRCC*, a string-based quantum-chemical program suite.[35] Several Dunning correlation-consistent fluorine basis sets [double-ζ (aug-cc-pVDZ), triple-ζ (aug-cc-pVTZ), quadruple-ζ (aug-cc-pVQZ), and quintuple-ζ (aug-cc-pV5Z)] were used to evaluate the basis-set effects. Corrections for incompleteness of the basis-set size have been adjusted by using the correlation-consistent basis sets, which can be extrapolated to the complete basis set (CBS) limit using equation $E(l_{max}) = E_{CBS} + B/l_{max}^3$ (B is the average value of the two highest l_{max}).[36] Core−valence (CV) correction has been performed by using the aug-cc-pwCVXZ (X = D, T, Q, 5) basis sets at the CCSD(T) level. Anharmonic corrections of the vibrational spectra have been investigated at the CCSD-(T) level using the program package *ACESII*.[34] Contributions of basis-set superposition errors (BSSEs) to the energetics were estimated at all ab initio levels using of the aug-cc-pVTZ basis set. Scalar and spin−orbit relativistic effects have not been considered in this study. All species investigated have shown normal T_1 diagnostic values and can be treated by single reference methods.

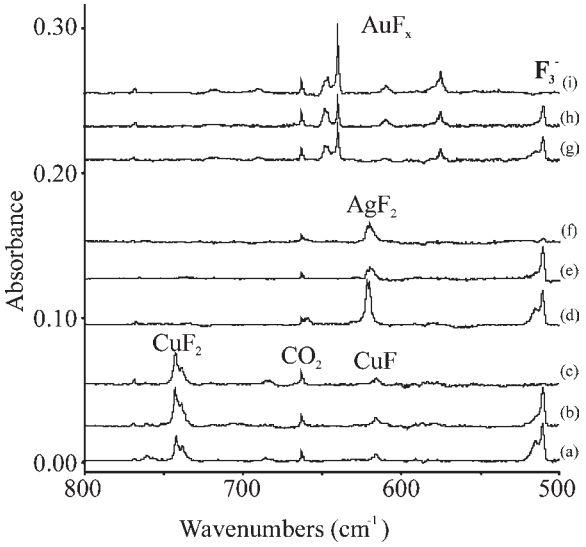

Figure 1. IR spectra for Cu, Ag, and Au atoms and F_2 reaction products in solid argon at 6 K: (a) Cu + F_2 (4% in argon) deposition for 60 min; (b) after > 290 nm irradiation for 15 min; (c) after > 220 nm irradiation for 15 min; (d) Ag + F_2 (4% in argon) deposition for 60 min; (e) after > 290 nm irradiation for 15 min; (f) after > 220 nm irradiation for 15 min; (g) Au + F_2 (4% in argon) deposition for 60 min; (h) after > 290 nm irradiation for 15 min; (i) after > 220 nm irradiation for 15 min.

Results and Discussion

Matrix-Isolation Experiments. A large number of laser-ablated metal [groups 3, 4, 11, and 13 (B, Al)] experiments were done with argon and neon samples containing molecular fluorine in order to prepare numerous metal fluoride molecules for matrix IR spectroscopic investigation, and these metal fluoride products will be identified elsewhere. Here we report one new IR absorption that is common, i.e., unshifted within experimental error, to these different metal experiments. These occur at 510.6 cm^{-1} in solid argon and 524.7 cm^{-1} in solid neon, and their metal-independent frequencies are suggestive of precursor electron capture products. Laser ablation of metals also produces electrons, and the electron flux depends on the electronic properties of the metal. Figures 1−3 illustrate representative spectra in solid argon and neon.

(25) Chertihin, G. V.; Citra, A.; Andrews, L.; Bauschlicher, C. W., Jr. *J. Phys. Chem. A* **1997**, *101*, 8793–8802.
(26) Burkholder, T. R.; Andrews, L. *J. Chem. Phys.* **1991**, *95*, 8697–8709.
(27) Frisch, M. J. T. G. W.; Schlegel, H. B.; Scuseria, G. E.; Robb, M. A.; Cheeseman, J. R.; Montgomery, J. A., Jr.; Vreven, T.; Kudin, K. N.; Burant, J. C.; Millam, J. M.; Iyengar, S. S.; Tomasi, J.; Barone, V.; Mennucci, B.; Cossi, M.; Scalmani, G.; Rega, N.; Petersson, G. A.; Nakatsuji, H.; Hada, M.; Ehara, M.; Toyota, K.; Fukuda, R.; Hasegawa, J.; Ishida, M.; Nakajima, T.; Honda, Y.; Kitao, O.; Nakai, H.; Klene, M.; Li, X.; Knox, J. E.; Hratchian, H. P.; Cross, J. B.; Bakken, V.; Adamo, C.; Jaramillo, J.; Gomperts, R.; Stratmann, R. E.; Yazyev, O.; Austin, A. J.; Cammi, R.; Pomelli, C.; Ochterski, J. W.; Ayala, P. Y.; Morokuma, K.; Voth, G. A.; Salvador, P.; Dannenberg, J. J.; Zakrzewski, V. G.; Dapprich, S.; Daniels, A. D.; Strain, M. C.; Farkas, O.; Malick, D. K.; Rabuck, A. D.; Raghavachari, K.; Foresman, J. B.; Ortiz, J. V.; Cui, Q.; Baboul, A. G.; Clifford, S.; Cioslowski, J.; Stefanov, B. B.; Liu, G.; Liashenko, A.; Piskorz, P.; Komaromi, I.; Martin, R. L.; Fox, D. J.; Keith, T.; Al-Laham, M. A.; Peng, C. Y.; Nanayakkara, A.; Challacombe, M.; Gill, P. M. W.; Johnson, B.; Chen, W.; Wong, M. W.; Gonzalez, C.; Pople, J. A. *Gaussian03*, revision C.02; Gaussian, Inc.: Wallingford, CT, 2004.
(28) Becke, A. D. *J. Chem. Phys.* **1993**, *98*, 5648–5652.
(29) Lee, C.; Yang, W.; Parr, R. G. *Phys. Rev. B* **1988**, *37*, 785–789.
(30) Miehlich, B.; Savin, A.; Stoll, H.; Preuss, H. *Chem. Phys. Lett.* **1989**, *157*, 200–206.
(31) Becke, A. D. *Phys. Rev. A* **1988**, *38*, 3098–3100.
(32) Perdew, J. P. *Phys. Rev. B* **1986**, *33*, 8822–8824.
(33) Werner, H.-J.; Knowles, P. J.; Lindh, R.; Manby, F. R.; Schütz, M.; Celani, P.; Korona, T.; Rauhut, G.; Amos, R. D.; Bernhardsson, A.; Berning, A.; Cooper, D. L.; Deegan, M. J. O.; Dobbyn, A. J.; Eckert, F.; Hampel, C.; Hetzer, G.; Lloyd, A. W.; McNicholas, S. J.; Meyer, W.; Mura, M. E.; Nicklass, A.; Palmieri, P.; Pitzer, R.; Schumann, U.; Stoll, H.; Stone, A. J.; Tarroni, R.; Thorsteinsson, T. *MOLPRO 2006.1, a package of ab initio programs*; Birmingham, U.K., 2006.
(34) Stanton, J. F.; Gauss, J.; Watts, J. D.; Szalay, P. G.; Bartlett, R. J.; Auer, A. A.; Bernholdt, D. E.; Christiansen, O.; Harding, M. E.; Heckert, M.; Heun, O.; Huber, C.; Jonsson, D.; Jusélius, J.; Lauderdale, W. J.; Metzroth, T.; Michauk, C.; Price, D. R.; Ruud, K.; Schiffmann, F.; Tajti, A.; Varner, M. E.; Vázquez, J.; Almlöf, J.; Taylor, P. R.; Helgaker, T.; Jensen, H. J. A.; Jørgensen, P.; Olsen, J. *ACESII*; ACESII: Mainz, Germany, 1992.
(35) Kállay, M.; Surján, P. R. *J. Chem. Phys.* **2001**, *115*, 2945.
(36) Halkier, A.; Helgaker, T.; Jorgensen, P.; Klopper, W.; Koch, H.; Olsen, J.; Wilson, A. K. *Chem. Phys. Lett.* **1998**, *286*, 243–252.

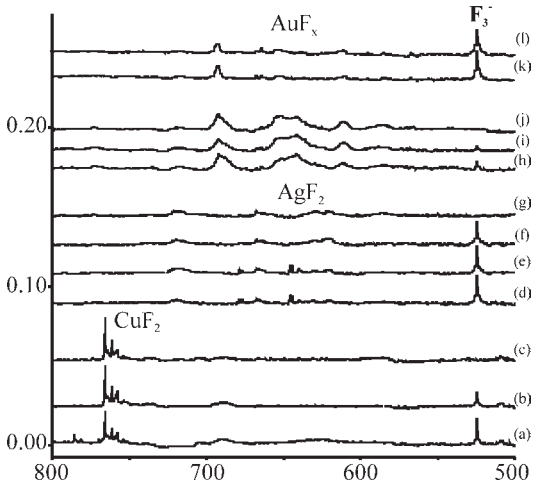

Figure 2. IR spectra for Cu, Ag, and Au atoms and F_2 reaction products in solid neon at 6 K: (a) Cu + F_2 (4% in neon) deposition for 60 min; (b) after > 290 nm irradiation for 15 min; (c) after > 220 nm irradiation for 15 min; (d) Ag + F_2 (4% in neon) deposition for 60 min; (e) after > 470 nm irradiation for 15 min; (f) after > 290 nm irradiation for 15 min; (g) after > 220 nm irradiation for 15 min; (h) Au + F_2 (4% in neon) deposition for 60 min; (i) after > 290 nm irradiation for 15 min; (j) after > 220 nm irradiation for 15 min; (k) Au + F_2 (2% in neon) deposition for 60 min; (l) after > 290 nm irradiation for 15 min.

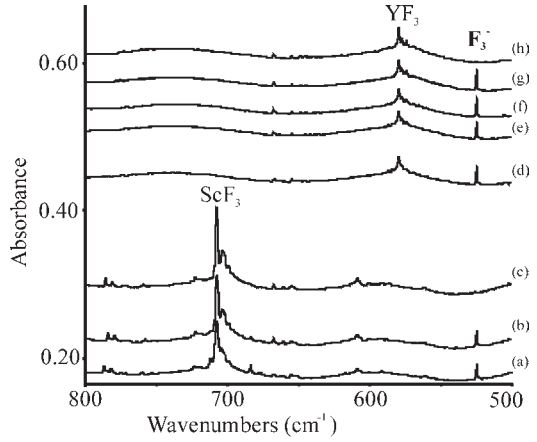

Figure 3. IR spectra for Sc and Y atoms and F_2 reaction products in solid neon at 6 K: (a) Sc + F_2 (0.5% in neon) deposition for 60 min; (b) after > 290 nm irradiation for 15 min; (c) after > 220 nm irradiation for 15 min; (d) Y + F_2 (0.5% in neon) deposition for 60 min; (e) after > 530 nm irradiation for 15 min; (f) after > 380 nm irradiation for 15 min; (g) after > 290 nm irradiation for 15 min; (h) after > 220 nm irradiation for 15 min.

IR spectra for the reaction products of Cu, Ag, and Au atoms and F_2 in solid argon at 6 K are compared in Figure 1. The new 510.6 cm^{-1} band sharpened upon irradiation at > 290 nm, as a blue shoulder decreased, and disappeared upon irradiation at > 220 nm. The corresponding neon matrix spectra are given in Figure 2. With copper, mercury arc irradiation at > 290 nm halves the new 524.7 cm^{-1} band, and finally irradiation at > 220 nm removed the new 524.7 cm^{-1} band. With silver, different irradiations were employed: irradiation at > 470 nm shows almost no changes, irradiation at > 290 nm decreases the band, and irradiation at > 220 nm destroys the new 524.7 cm^{-1} band. With gold, different fluorine concentrations were employed: the 524.7 cm^{-1} absorption is about the same intensity at higher concentrations (4%), but a lower concentration (2%) produced 4 times as much of the new 524.7 cm^{-1} band. Irradiation at > 290 nm had the same effect as before. The neon matrix spectrum for Sc and Y atoms in Figure 3 shows a similar behavior on the product yield. Irradiation at > 380 nm increased the 524.7 cm^{-1} band by 10%, and the next irradiation at > 290 nm increased the 524.7 cm^{-1} band again by another 5%. The final irradiation at > 220 nm shows no absorption remaining.

Assignments. The absorptions at 510.6 cm^{-1} in the argon matrix and at 524.7 cm^{-1} in the neon matrix are photosensitive upon irradiation at > 290 nm, which is consistent with their assignment to an isolated anion. These bands are below the $[M]^+[F_3]^-$ antisymmetric trifluoride stretching frequency of 550 cm^{-1} in an argon matrix, which is the typical relationship for cation−anion complexes and isolated anions. The $[NO_2]^-$ and $[BO_2]^-$ anions are cases in point where the cation complex absorptions are higher. Thus, $[NO_2]^-$ absorbs near 1275 cm^{-1} in crystalline solids and at 1244 cm^{-1} when isolated in a solid argon matrix, and the $[M]^+[BO_2]^-$ ion pairs exhibit bands at 1976−1946 cm^{-1}, whereas the isolated $[BO_2]^-$ anion fundamentally occurs at 1931 cm^{-1} in solid argon.[26,37] The best calculated gas-phase frequency of the isolated $[F_3]^-$ anion is 512 cm^{-1} at QCISD(T)[14] and 529.4 cm^{-1} at CCSD(T)/aug-cc-pVTZ, (this work), pointing to a lower frequency than the observed 550 cm^{-1} $[M]^+[F_3]^-$ value. The 510.6 cm^{-1} argon matrix and 524.7 cm^{-1} neon matrix absorptions are assigned here to the isolated trifluoride anion in media of different polarizabilities.

Structures. Figure 4 shows the optimized structures of polyfluoride anions at different levels of theory for, F_2, $[F_2]^-$, $[F_3]^-$, and $[F_5]^-$. The $[F_3]^-$ anion is calculated to show on each level used $D_{\infty h}$ symmetry. This is in agreement with previous observations and calculations. Unfortunately, no experimental bond length is known for this species. Therefore, our quantum-chemical calculations should represent the most reliable bond length for the $[F_3]^-$ anion, which is 173.2 pm at CCSD(T)/aug-cc-pV5Z level; see Table 1. Because the aim of this study is the investigation of $[F_3]^-$ and the higher polyfluoride anions, utilization of the aug-cc-pV5Z basis set is not cost-efficient. Therefore, we have used the aug-cc-pVTZ basis set for our productive work. This basis set shows less than 1 pm bond length error compared to the aug-cc-pV5Z basis set; see Table 1.

Other levels of theory, like DFT (BP86 and B3LYP), MP2, or CCSD, are unfortunately not accurate enough to describe higher polyfluoride molecules. This outcome is well-known and is illustrated by the nontrivial description of F_2 and its properties, such as the bond distance, frequency, and thermochemistry. Therefore, we use the most cost-efficient methodology of CCSD(T)/aug-cc-pVTZ to investigate these higher polyfluoride anions.

At this computational level, we found the open-shell $[F_4]^-$ to be a linear molecule with $D_{\infty h}$ symmetry (Figure 4). The computed bond lengths show two bonds with 175.3 pm and one with 179.0 pm, indicating two coordinated F_2 fragments.

For the pentafluoride anion, we found only one C_s-symmetrical minimum ("hockey stick" in Figure 4). This species can be described as a $[F_3]^-$ anion with an associated F_2 in the terminal position. The computed distance at the

(37) Milligan, D. E.; Jacox, M. E.; Guillory, W. A. *J. Chem. Phys.* **1970**, *52*, 3864–3868.

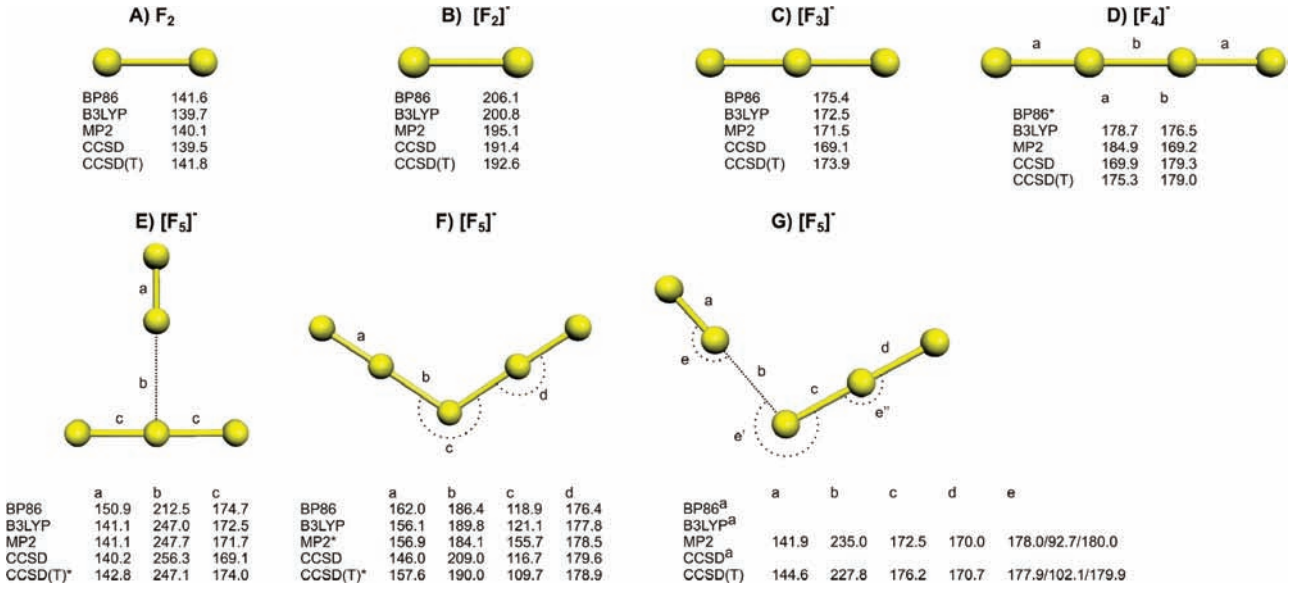

Figure 4. Polyfluoride anions optimized at different levels of theory using the aug-cc-pVTZ basis set: (*) no optimized minimum; (superscript a) optimization leading to the V-shaped structure F.

Table 1. Optimized Structures of Fluorine Species Computed at the CCSD(T) Level Using Different Basis-Set Sizes

structure	aug-cc-pVDZ	aug-cc-pVTZ	aug-cc-pVQZ	aug-cc-pV5Z
F_2	145.0	141.8	141.3	141.1
$[F_2]^-$	194.0	192.6	192.0	191.8
$[F_3]^-$ [a]	176.8	173.9	173.3	173.2
$[F_4]^-$ a	178.6	175.3	174.7	174.5
$[F_4]^-$ b	181.0	179.0	178.6	178.5
$[F_5]^-$ a	151.5	144.6	144.1	
$[F_5]^-$ b	210.4	227.8	227.4	
$[F_5]^-$ c	180.2	176.2	175.7	
$[F_5]^-$ d	171.8	170.7	170.2	
$[F_5]^-$ e	178.0/106.2/179.5	177.9/102.1/179.9	178.3/101.7/179.9	

[a] Other computed bond lengths: MCSCF(6,4)+MP2/TZ+2P, 174.9 pm;[21] MCSCF(7,8)+MP2/TZ+2P, 176.1 pm;[21] ACCD/TZP, 170.1 pm;[15] MP2/631+G*, 173.8 pm;[16] QCISD(T)/TZ2Pf+, 174.3 pm;[17] QCISD/D95V+*, 172.1 pm;[22] MP2/D95V+*, 173.3 pm;[22] BLYP/aug-cc-pVTZ, 177.5 pm;[22] B3LYP/aug-cc-pVTZ, 172.5 pm[22] CCSD(T)/aug-cc-pVTZ, 173.9 pm;[24] MRCI/aug-cc-pVQZ, 173.8 pm[23]

CCSD(T) level between these two fragments is 227.8 pm, which lies within the sum of the van der Waals radii of fluorine. The bond length of the aggregated F_2 unit is slightly elongated compared to the free F_2 molecule (Figure 4G, bond a). Such a bond elongation of 2.3 pm is also observed for the connecting F atom of the $[F_3]^-$ anion (bond c in Figure 4G). In contrast, bond d of this species is shortened by 3.2 pm compared to the free $[F_3]^-$ anion calculated at the CCSD(T) level. Other isomers of the $[F_5]^-$ anion, computed at the CCSD(T)/aug-cc-pVTZ level, optimized to transition states or higher saddle points on the potential energy surface and therefore were higher in energy (see Figure 5). Note that structure optimizations of the $[F_5]^-$ anion using the CCSD(T) "hockey stick" minimum structure as the starting point always led to minimum V-shaped structures at the CCSD, B3LYP, and BP86 levels. This V-shaped (C_{2v}) structure is commonly observed for other pentahalogen anions like

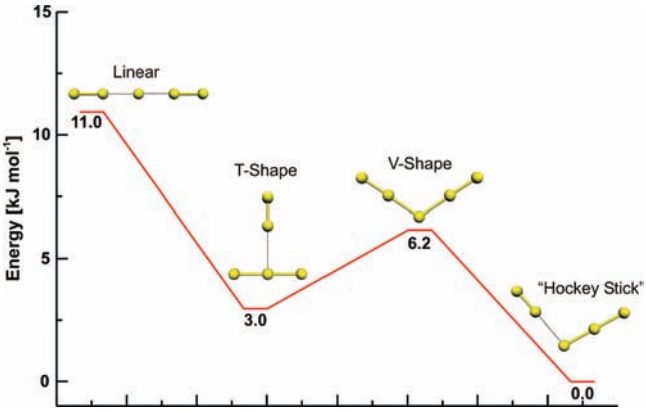

Figure 5. Optimized structures of $[F_5]^-$ isomers at the CCSD(T)/aug-cc-pVTZ level. All higher-energy structures are computed to be transition states or saddle points on the hypersurface.

$[I_5]^-$[38] or $[Br_5]^-$.[39,40] Only the MP2 method also led to a "hockey stick" structure that was similar to that of the CCSD(T) one (Figure 4).

Thermochemical Stability. Our computed bond dissociation energies of the $[F_3]^-$ anion are in very good agreement with the experimentally measured values. They have been determined from energy-resolved collision-induced dissociation cross-sectional measurements in two tandem mass spectrometers.[14] The unimolecular gas-phase F_2 elimination $[F_3]^- \rightarrow [F]^- + F_2$ is calculated to be 99.5 kJ mol^{-1} at the CCSD(T)/aug-cc-pVTZ level and is therefore in excellent agreement with the experimental value of 98.4 ± 10.6 kJ mol^{-1}. Although the calculation of the homolytic bond breaking $[F_3]^- \rightarrow F + [F_2]^-$ shows a deviation of 11.4 kJ mol^{-1} from the experimental value of 125.4 ± 12.5 kJ mol^{-1}, it is still within the experimental error of 12.5 kJ mol^{-1}.[14] Moreover, several corrections have to be considered if thermochemistry is to achieve at an accuracy on the order of ±1 kcal mol^{-1}. The first correction accounts for the

(38) Sharp, S. B.; Gellene, G. I. *J. Phys. Chem. A* **1997**, *101*, 2192–2197.
(39) Schuster, P.; Mikosch, H.; Bauer, G. *J. Chem. Phys.* **1998**, *109*, 1833–1844.
(40) Nizzi, K. E.; Pommerening, C. A.; Sunderlin, L. S. *J. Phys. Chem. A* **1998**, *102*, 7674–7679.

Table 2. Reaction Energies of Fluorine Species Computed at the CCSD(T) Level Using Different Basis-Set Sizes

reaction (kJ mol^{-1})	(a) $F_2 \rightarrow 2F$	(b) $[F_2]^- \rightarrow F + [F]^-$	(c) $[F_3]^- \rightarrow F_2 + [F]^-$	(d) $[F_3]^- \rightarrow [F_2]^- + F$	(e) $[F_4]^- \rightarrow [F_2]^- + F_2$	(f) $[F_4]^- \rightarrow [F_3]^- + F$	(g) $[F_5]^- \rightarrow [F_3]^- + F_2$	(h) $[F_5]^- \rightarrow [F]^- + 2F_2$
				aug-cc-pVDZ				
ΔE_{elec}	125.5	114.4	117.9	128.9	29.1	25.6	22.1	140.0
ΔE_{CV}[a]	0.54	0.21	−0.27	0.05	−0.73	0.35	0.05	−0.22
$\Delta E_{ZPE(harmonic)}$	4.94	2.71	2.24	4.47	1.6	0.6	3.0	5.3
$\Delta E_{ZPE(anharmonic)}$	4.91	2.70	2.17	4.38			2.7	4.9
ΔH[b]	120.1	111.5	116.0	124.5	28.2	24.7	24.8	145.1
				aug-cc-pVTZ				
ΔE_{elec}	153.1	115.8	99.5	136.8	12.8	29.1	18.0	117.5
ΔE_{CV}[a]	−0.24	−0.07	−0.69	−0.86	−1.62	−0.84	−0.12	−0.81
$\Delta E_{ZPE(harmonic)}$	5.53	2.72	2.17	4.98	1.4	2.3	2.4	2.6
$\Delta E_{ZPE(anharmonic)}$	5.49	2.70	2.13	4.92				
ΔE_{BSSE}	5.0	2.4	2.1	4.7	3.2	1.8	1.0	3.1
ΔH[c]	142.9	110.8	96.0	128.0	9.8	25.8	16.5	117.2
				aug-cc-pVQZ				
ΔE_{elec}	158.3	117.1	98.3	139.5	11.7	30.6	17.4	115.7
ΔE_{CV}[a]	−0.32	−0.12	−0.79	−1.00	−1.28	−0.63		
$\Delta E_{ZPE(harmonic)}$	5.55	2.71	1.71	4.55	1.5	0.9		
$\Delta E_{ZPE(anharmonic)}$	5.51	2.69	1.67	4.49				
ΔH[b]	153.1	114.5	97.4	136.0	8.9	29.1		
				aug-cc-pV5Z				
$\Delta E_{elec.}$	160.0	117.1	96.9	139.7	10.3	30.6		
ΔE_{CV}[a]	−0.34	−0.12	−0.81	−1.03				
$\Delta E_{ZPE(harmonic)}$	5.57	2.73						
$\Delta E_{ZPE(anharmonic)}$	5.54	2.71						
ΔH[b]	154.8	114.5	97.7	140.7				
				CBS[d]				
ΔE_{CBS}	161.7	117.1	95.4	140.0	8.5	31.0	16.3	108.0
ΔH[e]	156.5	114.5	94.5	136.5	5.7	29.5		
				Exptl				
	154.4[42]	116.8 ± 6.7[43]	98.4 ± 10.6[14]	125.4 ± 12.5[14]				

[a] Values are CV-corrected using the aug-cc-pwCVXZ (X = D, T, Q, 5) basis sets. [b] $\Delta H = \Delta E_{elec} - \Delta E_{CV} + \Delta E_{ZPE(anharmonic\ or\ harmonic)}$. [c] $\Delta H = \Delta E_{elec} - \Delta E_{CV} + \Delta E_{ZPE(anharmonic\ or\ harmonic)} + \Delta E_{BSSE}$. [d] Estimation of the CBS limit by using equation $E(l_{max}) = E_{CBS} + B/l_{max}^3$ (B is the average value of the two highest l_{max}); more details are shown in the Supporting Information.[36] [e] $\Delta H = \Delta E_{CBS} - \Delta E_{CV} + \Delta E_{ZPE(anharmonic)}$ values of ΔE_{CV} and $\Delta E_{ZPE(anharmonic)}$ are taken from aug-cc-pVQZ, except for $[F_4]^-$, where $\Delta E_{ZPE(harmonic)}$ was used.

incompleteness of the basis-set size and can be adjusted by using the correlation-consistent basis sets aug-cc-pVXZ, which can be extrapolated to the CBS limit (Table 2). This effect accounts for both reactions of the $[F_3]^-$ anion having less than 1 kJ mol^{-1}. The second effect that has to be considered is the CV correction. Usually, electronic structure calculations invoke the frozen-core approximation, where the 1s orbital, e.g., in fluorine, is not taken into account for the electron correlation. The CV correction has been performed by using the aug-cc-pwCVXZ (X = D, T, Q, 5) basis sets at the CCSD(T) level and is computed to be less than 2 kJ mol^{-1} for all investigated reactions in this study (Table 2 and the Supporting Information). Furthermore, we have to correct for the zero-point energy (ZPE), which is usually computed as a harmonic treatment, neglecting the anharmonic contributions. However, to be as exact as possible, anharmonic ZPEs are given in Table 2. Considering all of these corrections, the reactions $[F_3]^- \rightarrow [F]^- + F_2$ and $[F_3]^- \rightarrow F + [F_2]^-$ show ΔH values of 94.5 and 136.5 kJ mol^{-1}, respectively, which are in good agreement with the experimentally determined values; see Table 2. Note, the only method that shows reliable agreement with the experimental determind values is the coupled-cluster (CCSD(T)) method (Table 4).

For the tetrafluoride anion, we have computed the concerted F_2 elimination $[F_4]^- \rightarrow [F_2]^- + F_2$ and the homolytic bond breaking $[F_3]^- \rightarrow F + [F_2]^-$. Both dissociation channels show endothermic eliminations of 11.4 and 26.8 kJ mol^{-1}, respectively (Table 2).

On the basis of these findings, the stability of the $[F_5]^-$ anion ("hockey stick") has been investigated. Scanning the potential energy surface by stepwise elongation of the $F_2 \cdots [F_3]^-$ bond distance leads to a barrier of 19.3 kJ mol^{-1} at the CCSD(T) level (Figure 6). The corresponding elimination of F_2 from $[F_5]^-$ to form the known $[F_3]^-$ anion is computed to be endothermic by 18.0 kJ mol^{-1} at the CCSD(T)/aug-cc-pVTZ level. Taking CV corrections (ΔE_{CV} −0.12 kJ mol^{-1}), zero-point energy correction ($\Delta E_{ZPE(harmonic)}$ 0.9 kJ mol^{-1}), and BSSE (1.0 kJ mol^{-1}) of the $[F_5]^- \rightarrow [F_3]^- + F_2$ elimination into account, the energy is only negligibly lowered by 1.5 kJ mol^{-1}. The second possible decomposition channel, $[F_5]^- \rightarrow [F]^- + 2F_2$, shows an even more endothermic reaction of 117.5 kJ mol^{-1}. ΔE_{CV} (−0.81 kJ mol^{-1}), $\Delta E_{ZPE(harmonic)}$ (−2.6 kJ mol^{-1}), and ΔE_{BSSE} (3.1 kJ mol^{-1}) of this reaction are computed to be 0.3 kJ mol^{-1}. These endothermic unimolecular decomposition channels, together with the computed "barrier", account for the stability of this polyfluoride anion and support speculation of the previous observations

Table 3. Harmonic and Anharmonic Frequencies of Fluorine Species Computed at the CCSD(T) Level Using Different Basis-Set Sizes

frequencies[a]	$\nu_{1(\text{Harm.})}$	Int.	$\nu_{1(\text{Anh.})}$	$\nu_{2(\text{Harm.})}$	Int.	$\nu_{2(\text{Anh.})}$	$\nu_{3(\text{Harm.})}$	Int.	$\nu_{3(\text{Anh.})}$	ν_4	Int.	$\nu_{4(\text{Anh.})}$	ν_5	Int.	$\nu_{5(\text{Anh.})}$
							(a) F_2								
aug-cc-pVDZ	826.7		803.0												
aug-cc-pVTZ	924.2		900.8												
aug-cc-pVQZ	927.3		904.5												
aug-cc-pV5Z	931.6		908.6												
exptl	916.64[42]														
							(b) $[F_2]^-$								
aug-cc-pVDZ	453.7		441.9												
aug-cc-pVTZ	455.1		442.7												
aug-cc-pVQZ	453.3		441.2												
aug-cc-pV5Z	456.3		443.9												
exptl	460[44]														
							(c) $[F_3]^-$								
		PIu			SGg^+			SGu^-							
aug-cc-pVDZ	242.7	47	233.4	380.9		371.3	578.2	734	545.6						
aug-cc-pVTZ	257.4	49	252.1	406.4		396.5	552.6	946	529.1						
aug-cc-pVQZ	259.4	49	254.0	407.1		397.0	546.8	961	523.4						
aug-cc-pV5Z	258.1[b]			406.5[b]			546.9[b]								
exptl				461[11]			550,[11] 525[tw]								
							(d) $[F_4]^-$								
aug-cc-pVDZ	101.2	11		179.1			283.8			323.2	453		516.1		
aug-cc-pVTZ	108.2	10		191.7			302.3			330.6	484		499.4		
aug-cc-pVQZ [b]	106.3			192.8			285.9			449.0			509.22		
							(e) $[F_5]^-$[c]								
		A″			A′			A′			A′			A′	
aug-cc-pVDZ	248.1	4	241.4	258.1	54	246.6	395.5	5	381.9	484.9	812	368.0	629.4	83	549.7
aug-cc-pVTZ	260.0	3		266	5		413.6	10		527.5	639		805.0	76	

[a] Harmonic and anharmonic frequencies in cm^{-1}; intensities in km mol^{-1}. [b] Harmonic frequencies calculated with the program *MOLPRO*. [c] Low vibrational frequencies (under 200 cm^{-1}): aug-cc-pVDZ, 188.4 (0), 188.1 (0), 119.3 (217), 25.6 (7); aug-cc-pVTZ, 146.6 (1), 145.8 (0), 124.8 (20), 16.0 (8)

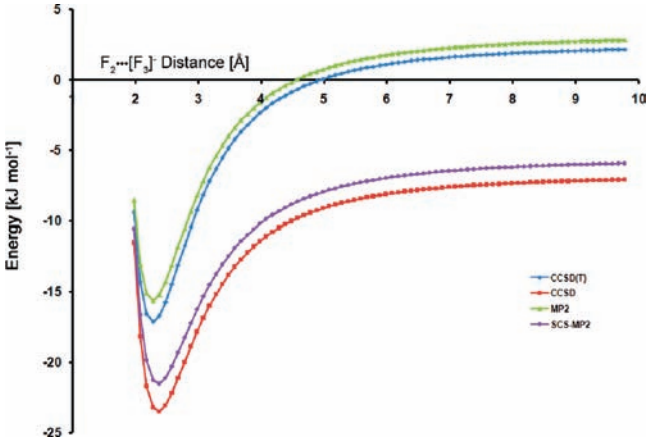

Figure 6. CCSD(T) scan of the potential energy surface by stepwise elongation (0.1 Å per step) of the $F_2\cdots[F_3]^-$ bond distance, starting from a bond distance of 1.878 Å.

in a flowing afterglow source of an energy-resolved collision-included dissociation cross-sectional measurement in a tandem mass spectrometer where a corresponding $[F_5]^-$ peak (m/z 95) was indicated in the gas phase.[14]

Frequencies. It is known that the exact calculation of F_2 frequencies is still no easy task and the application of sophisticated methods is necessary. It was reported that even the CCSD(T) method shows intrinsic errors, which are significantly larger than usually thought. Indeed, our CCSD(T)/aug-cc-pV5Z anharmonic frequency calculation still shows a $\Delta\nu$ of 8 cm^{-1} compared to the experimentally determined value (Table 3). The same difference of 8 cm^{-1} is observed for harmonic frequency treatment at the CCSD(T)/aug-cc-pVTZ level, whereas larger basis sets decrease the improvement (Table 3). This observation is mainly due to error cancellations incurred by truncation of the coupled-cluster hierarchy as in the case of the CCSD(T) description by approximation of the connected triples through perturbative treatment and disregard of higher-order connected excitations. The application of higher-order excitations like CCSDT, CCSDT(Q), etc., would improve this discrepancy. However, the aim of this study is the investigation of polyfluoride anions, and therefore the application of these higher-order coupled-cluster calculations is computationally too expensive.

However, the $[F_3]^-$ species has its highest computed harmonic IR band at 546.8 cm^{-1} by the CCSD(T)/aug-cc-pVQZ level. As we have already reported above, the free anionic species $[F_3]^-$ shows its highest frequency mode at 524.7 cm^{-1} in neon matrixes and 510.6 cm^{-1} in argon matrixes. This difference of 26.3 cm^{-1} between the calculated frequency and the experimental band in neon is due in large part to the harmonic calculation treatment of this system. Anharmonic correction at the CCSD(T) level using the aug-cc-pVTZ and -QZ basis set gives an anharmonic correction of 23.5 cm^{-1}, leading to a vibrational mode at 523.4 cm^{-1}. This is in very good agreement with the free anionic band at 524.7 cm^{-1} in neon, which is also subject to some weak matrix interaction. The 14.1 cm^{-1} red-shifted band in argon matrixes is due to stronger

Table 4. Reaction Energies of Fluorine Species Computed at Different Levels of Theory Using the aug-cc-pVTZ Basis-Set Size[a]

reaction	BP86	B3LYP	MP2	CCSD	CCSD(T)	CCSDT	exptl
(a) $F_2 \rightarrow 2\ F$	219.0	155.3	173.6	124.5	153.1	151.4	154.4[42]
	6.0	*6.3*	*6.0* (5.3)	*6.0* (5.5)	*5.5* (5.0)		
(b) $[F_2]^- \rightarrow F + [F]^-$	201.8	167.7	139.5	102.2	115.8		116.8 ± 6.7[43]
	1.8	*2.1*	*2.5* (2.2)	*2.8* (2.3)	*2.7* (2.4)		
(c) $[F_3]^- \rightarrow F_2 + [F]^-$	179.2	132.5	97.0	51.1	99.5		98.4 ± 10.6[14]
	0.9	*0.7*	*2.5* (2.05)	*0.3* (2.1)	*1.7* (2.1)		
(d) $[F_3]^- \rightarrow [F_2]^- + F$	196.5	120.1	131.1	73.4	136.8		125.4 ± 12.5[14]
	5.0	*4.8*	*6.0* (5.2)	*3.6* (5.3)	*4.5* (4.7)		
(e) $[F_4]^- \rightarrow [F_2]^- + F_2$		51.1	68.8	−39.7	12.8		
		1.1	*-4.3* (2.9)	*-2.5* (2.5)	*-1.4* (3.2)		
(f) $[F_4]^- \rightarrow [F_3]^- + F$		86.3	111.3	11.4	29.1		
		-0.3	*-4.3* (11.9)	*-4.9* (4.4)	*-2.3* (1.8)		
(g) $[F_5]^- \rightarrow [F_3]^- + F_2$	65.9	35.1	16.2	17.0	18.0		
	3.9	*3.1*	*1.2* (0.9)	*2.4* (0.8)	*0.9* (1.0)		
(h) $[F_5]^- \rightarrow [F]^- + 2F_2$	245.1	167.5	113.2	68.1	117.5		
	4.8	*3.8*	*3.7* (3.0)	*2.8* (2.9)	*2.6* (3.1)		

[a] Reaction in parenthesis at SCS-MP 87.9 kJ mol^{-1}; values in italic are ZPE corrections, and values in parentheses are BSSE corrections.

interaction with the more polarizable matrix host (see below).

In the case of the polyfluoride anion $[F_5]^-$, we have computed two intense harmonic bands above 200 cm^{-1}, the first one at 805 cm^{-1} (68 km mol^{-1}) and the second band at 527 cm^{-1} (769 km mol^{-1}) (Table 3). Unfortunately, we were not able to compute anharmonic corrections of this molecule because of a lack of computational resources. However, the calculated frequencies support our description of the $[F_5]^-$ anion as a $[F_3]^-$ ion indicated by the 527 cm^{-1} band and a coordinated F_2 molecule showing a perturbed F−F stretching band at 805 cm^{-1}. Because of the weak interaction between F_2 and $[F_3]^-$, it is of interest to determine how strong the influence of the matrix host argon or neon is (see below).

Noble Gas Influences

In principle, matrix-isolation comprises a category of experimental techniques in which guest molecules or atoms are trapped in rigid host materials. Usually, it is preferable that the host material does not interact with the guest molecules to simulate pseudo-gas-phase conditions. A host material that is known to have only minor interactions with the trapped guest species is the solid noble gas neon. Nevertheless, even this host material has some minor interactions that can be competitive with the species in question, especially if the guest molecule is fragile like $[F_5]^-$.

To evaluate the influence of the noble gas atoms on the polyfluoride anions, we have computed interaction energies at various ab initio levels. Three minimum structures have been found at the CCSD(T)/aug-cc-pVTZ level of the $Ng[F_3]^-$ (Ng = Ne, Ar) species (Figure 7). The linear C_{2v}-symmetrical species A was only found to be a minimum for the $Ar[F_3]^-$ species. The Ar−F bond distance is calculated to be 306.6 pm, which is below the sum of the van der Waals radii of 320 pm. The second minimum structure, which was also found to be a minimum for the $Ne[F_3]^-$ species, shows C_s symmetry and is 2.8 kJ mol^{-1} lower in energy than species A at the CCSD(T) level. In this case, the $Ar[F_3]^-$ species has a Ar−F bond length below the sum of the van der Waals radii, whereas the $Ne[F_3]^-$ bond distance of 296.3 is beyond the value of 290 pm, indicating the weak coordination of the Ne atom. These pseudo-T-shaped structures show a small distortion from C_{2v} symmetry of less than 3° (Figure 7). Both argon complexes show relatively large interaction energies for the argon elimination reaction $Ar[F_3]^- \rightarrow [F_3]^- + Ar$ of 5.6 and 8.5 kJ mol^{-1} at the CCSD(T) level for species A and B, respectively. The corresponding elimination reaction of the $Ne[F_3]^-$ complex shows only a negligible dissociation energy of 2.6 kJ mol^{-1} (ZPE-corrected value 1.0 kJ mol^{-1}). This suggests that neon has almost no influence on the guest species, whereas argon competes with a coordinated F_2 unit in, for example, $[F_5]^-$.

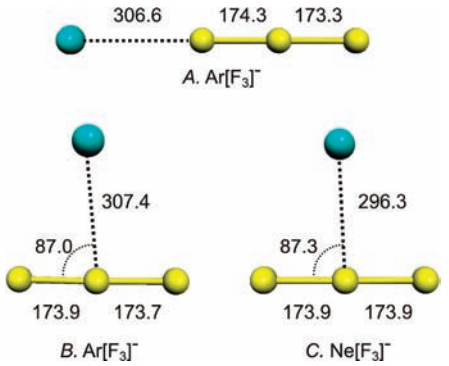

Figure 7. $Ng[F_3]^-$ (Ng = Ne, Ar) minimum structures optimized at the CCSD(T)/aug-cc-pVTZ level. Species A shows C_{2v}, and species B and C show C_s symmetry.

Figure 8 shows the potential energy surface scan of the $Ng\cdots[F_3]^-$ bond distance of the linear and T-shaped structures, indicating the larger interaction energies of argon relative to neon. Furthermore, it is shown that MP2 underestimates and CCSD and SCS-MP2 overestimate the interaction energies of the $Ar[F_3]^-$ complex in comparison to the CCSD(T) energy. Note that this trend is not observed for the $Ne[F_3]^-$ complex, in which all other methods overestimate the interaction energy.

One of the main aspects in using noble gas atoms like neon and argon in matrix-isolation spectroscopy is their weak interaction with the matrix guest. Nevertheless, these atoms also have an effect on the vibrational frequency of the guest

(41) Christe, K. O. *J. Fluorine Chem.* **1995**, *71*, 149–150.
(42) Huber, K. P.; Herzberg, G. *Molecular Spectra and Molecular Structure, 4: Constants of Diatomic Molecules*; Van Nostrand: New York, 1979; p 716.
(43) Wenthold, P. G.; Squires, R. R. *J. Phys. Chem.* **1995**, *99*, 2002–2005.
(44) Howard, W. F., Jr.; Andrews, L. *J. Am. Chem. Soc.* **1973**, *95*, 3045–3046.

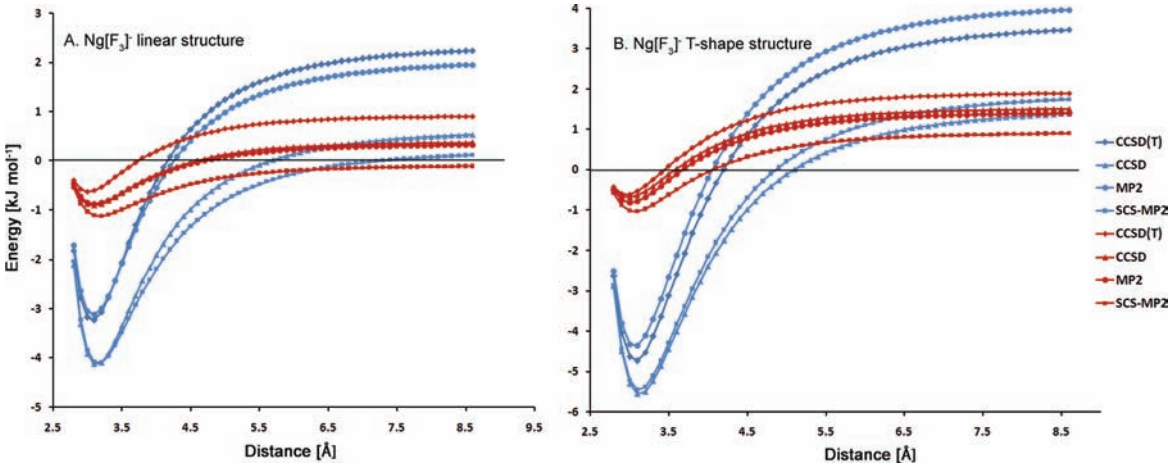

Figure 8. Scan of the potential energy surface by stepwise elongation (0.1 Å per step) of the Ng···$[F_3]^-$ bond distance of the linear and T-shaped structures at the CCSD(T), CCSD, MP2, and SCS-MP2 levels (starting from a bond distance of 2.8 Å). $Ne[F_3]^-$ and $Ar[F_3]^-$ complexes are denoted by red and blue lines, respectively.

Table 5. Calculation of the Harmonic Frequencies of $Ng[F_3]^-$ (Ng = Ne, Ar) Complexes[a]

frequency	$[F_3]^-$	$Ne[F_3]^-$ (T-shaped)	$Ar[F_3]^-$ (T-shaped)	$Ar[F_3]^-$ (linear)
ν_1		23.0	17.0	38.1
ν_2		56.0	65.7	62.1
ν_3		255.8	254.4	258.9
ν_4	260.9	258.9	266.7	258.9
ν_5	391.0	398.6	400.5	403.3
ν_6	550.8	549.8	554.0	550.4
ν_6		510.6[b]	524.7[c]	524.7[c]

[a] Calculations have been performed by *MOLPRO* using the FC-CCSD(T)/aug-cc-pVTZ level. [b] Experimental values in neon matrixes. [c] Experimental values in argon matrixes.

molecule. To consider this effect, we have investigated the influence of one noble gas atom, neon or argon, on the vibrational modes of the $[F_3]^-$ ion (Table 5). It is shown that the Ne atom has almost no influence, 1 cm^{-1}, on the antisymmetric stretching mode, whereas the Ar atom in the T-shaped structure shows a shift of 3.2 cm^{-1}. The influence of the Ng atoms increases for the symmetric stretch mode by 7.6 cm^{-1} for neon, 9.5 cm^{-1} for the T-shaped complex, and 12.3 cm^{-1} for the linear complex (Table 5). We have considered one Ng atom only in our calculations. In the matrix-isolation experiment, the guest molecule is surrounded by several host atoms and all of them have an influence on the observed band. This matrix host effect is well-known for argon and neon and leads sometimes even to blue-shifted bands. However, a detailed quantum-chemical investigation to estimate the whole "vacuum"-to-"noble gas" shift in such a host environment is out of the scope of the present study and will be considered elsewhere.

Bonding Analysis

Chemical bonding in hypervalent species like $[F_3]^-$ can be described as a three-center, four-electron bond (3c-4e). In principle, this can be viewed as a linear combination of atomic p orbitals that originate from all three F atoms, forming the hypervalent bond. The linear combination of these orbitals leads to the formation of three molecular orbitals that describe the hypervalent bonding. Figure 9 shows these orbitals, in which the electrons occupy the bonding and nonbonding

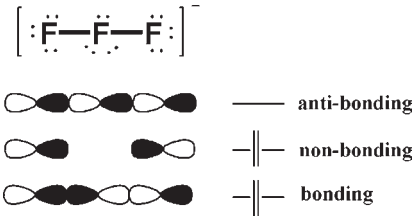

Figure 9. Linear combination of p orbitals leading to the formation of three molecular orbitals that describe hypervalent bonding in $[F_3]^-$.

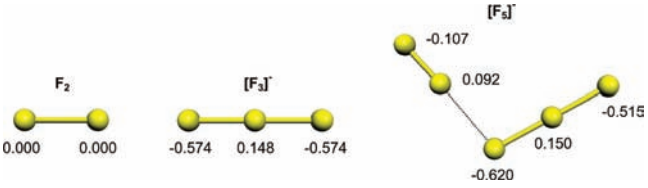

Figure 10. NPA at the B3LYP level for the polyfluoride anions.

orbitals. This arrangement indicates that most of the electron density should be located at the terminal F atoms. Indeed, our population analysis shows that the most negative natural population analysis (NPA) charges occur at the terminal atoms, where the central F atom is slightly positively charged (Figure 10). Analyzing the $[F_5]^-$ anion, we observe charge distributions similar to those in $[F_3]^-$, with a positive charge on the central atom (0.150) of the $[F_3]^-$ unit whereas the terminal atom is negatively charged by −0.515. The atom at the elbow is computed to be the most negative atom (−0.620), which has the positively charged F atom (0.092) of the F_2 ligand situated adjacent to it. This charge separation is consistent with the above-mentioned description in terms of a F_2 molecule coordinated to a $[F_3]^-$ species. Analysis of the F_2···$[F_3]^-$ bonding situation using the electron localization function shows indeed that the main contribution is of ionic character.

Conclusions

We have reported for the first time IR spectra of the isolated trifluoride anion $[F_3]^-$ stabilized under cryogenic conditions in neon and argon matrixes. These species were formed during the laser ablation of several metals (Cu, Ag, Au, Ti, Zr, Sc, and Y) with excess F_2 in neon and argon

at 4 K. The isolated trifluoride anion was observed in argon matrixes at 510.6 cm^{-1}, whereas IR absorptions at 524.7 cm^{-1} have been observed in neon matrixes independent of the metal employed. These bands are below the $[M]^+[F_3]^-$ ion-pair complex antisymmetric trifluoride stretching frequency of 550 cm^{-1} in solid argon, which is the typical relationship for cation−anion complexes and matrix-isolated anions. Quantum-chemical calculations up to and including the CCSD(T) level support the assignment of a free $[F_3]^-$ anion. Attempts to stabilize this anion as ion-pair complex $[N(CH_3)_4]^+[F_3]^-$ were not successful.[13,41] Furthermore, it is shown by state-of-the-art quantum-chemical calculations that $[F_5]^-$ is indeed a thermochemically stable species and therefore confirms speculation about a possible $[F_5]^-$ signal in the flowing afterglow source of a mass spectrometry experiment. The species can be described as a $[F_3]^-$ anion with a terminally coordinated F_2 molecule. With this experimental observation at hand, F_2 is shown to be a possible ligand under cryogenic conditions.

Acknowledgment. The authors are grateful to M. Kaupp and I. Krossing for kindly providing computational resources and D. Himmel and C. Knapp for fruitful discussions. S.R. thanks the Fonds der Chemischen Industrie and the Alexander von Humboldt Foundation for financial support. X.W. thanks the support from NNSFC (20973126). L.A. acknowledge support from the National Science Foundation.

Supporting Information Available: Estimation of the CBS (Table 1). This material is available free of charge via the Internet at http://pubs.acs.org.